be possible to achieve this type of equilibrium. This gives us first, a method of measuring δ_∞ which does not depend upon having an initially space charge free crystal. Second, by applying low fields to the crystal, we can measure directly the dependence of j_0 (at equilibrium) upon field strength. This same dependence may not hold, of course, for the ordinary temperatures at which the crystal is usually operated, but the information should none the less be theoretically valuable.

Finally, at ordinary temperatures, j_0 can be measured as a function of F_0, and the results used in Eq. (27) to determine j_0 as a function of $F(0)$. This is not a direct measure of $F(0)$, however, and should preferably be supplemented by other measurements.

We have emphasized the determination of j_0 as a function of $F(0)$ because it seems to us a good way of getting some information as to what goes on inside the plasma layer.

We are considerably indebted to various of our colleagues, particularly to Dr. R. W. Hamming, for a discussion of mathematical methods, and to Drs. McKay and Ahearn for extensive discussions of their experiments, and the bearing of the present theory upon them.

The data which we used in preparing Figs. 3 and 4 are from McKay's preliminary data, and are being carefully checked by him for later publication. It is thought that these data, although preliminary, are nearly enough correct so that use of the final data will not appreciably alter the theory or the conclusions drawn from it.

PHYSICAL REVIEW VOLUME 75, NUMBER 2 JANUARY 15, 1949

Absolute Voltage Determination of Three Nuclear Reactions

R. G. HERB, S. C. SNOWDON, AND O. SALA
University of Wisconsin, Madison, Wisconsin

(Received September 23, 1948)

A large electrostatic analyzer was used in conjunction with the Wisconsin electrostatic generator for an absolute voltage determination of the $Li^7(pn)Be^7$ threshold, an $Al^{27}(p\gamma)Si^{28}$ resonance, and a $F^{19}(p\alpha', \gamma)O^{16}$ resonance. Using absolute volts the values found are 1.882 Mev, 0.9933 Mev, and 0.8735 Mev, respectively. The uncertainties in the measurements appear to be about ± 0.1 percent.

INTRODUCTION

AN absolute measurement of the proton energy at the Li($p\gamma$) resonance was carried out by Hafstad *et al.*[1], using a calibrated resistor stack made up of I.R.C. metalized resistors. Parkinson *et al.*[2] checked this measurement and agree on a value of 0.440 Mev for the resonance energy with an estimated error of about two percent. Based on this determination, work at a number of laboratories lead to a number of secondary fixed points (i.e., F($p\gamma$) at 0.862 Mev and Li(pn) at 1.856 Mev), which are used widely as reference voltages. Recently Tangen[3] has measured the Li($p\gamma$) resonance by the method used in reference (1) and has obtained 0.440 Mev with an estimated uncertainty of $\frac{1}{2}$ percent.

If one attempts to establish absolute voltage values above 1 Mv, the resistor method becomes difficult. In this case some form of electrostatic analyzer can be used to scale down the voltage to be measured by a factor of about 100. Hanson and Benedict[4] used an electrostatic analyzer, calibrated by an electron beam, to determine the following reaction energies: Li(pn) at 1.883 Mev, Be(pn) at 2.058 Mev, F($p\gamma$) at 0.877 Mev, and Li($p\gamma$) at 0.4465 Mev. An absolute calibration by direct calculation from the geometry was also

[1] L. R. Hafstad, N. P. Heydenburg, and M. A. Tuve, Phys. Rev. **50**, 504 (1936).
[2] Parkinson, Herb, Bernet and McKibben, Phys. Rev. **53**, 642 (1938).
[3] R. Tangen, Kgl. Norske Vid. Sels. Skrifter (1946) NRI.
[4] A. O. Hanson and D. L. Benedict, Phys. Rev. **65**, 33 (1944).

used as a check. The absolute accuracy was thought to be about 0.3 percent.

At the University of Wisconsin a large 90° electrostatic analyzer was constructed in 1946[5] and has been in use for about two years. During this time excellent stability of equipment and reproducibility of results have been obtained. In this analyzer the plate separation is relatively large; therefore, an accurate measurement of the gap width is possible. Also, since the path length of the ion beam in the analyzer is about $1\frac{1}{2}$ meters, the end corrections are small. Finally, since the geometrical measurements depend only on a ratio of two distances, the analyzer is self-compensating for temperature variations.

Although the consistency of Hanson's work was quite satisfactory, the departure of $1\frac{1}{2}$ percent from the old values was disturbing. It was felt that another independent check should be made before shifting from the old Li 0.440-Mev standard. For the reasons indicated the Wisconsin equipment seemed well adapted for this purpose and hence was used to measure the Li(pn) threshold, the Al($p\gamma$) resonance which on the old scale was at 0.985 Mev, and the F($p\gamma$) resonance. Measurement of the analyzer voltage together with the analyzer geometry gives an absolute determination of the proton energy at these points. As a check on the dependability of the results, the analyzer geometry was changed substantially after one series of runs and all the measurements were repeated.

MEASUREMENT OF VOLTAGE ON ANALYZER PLATES

From Fig. 2 it is seen that the aperture limiting slit and the exit slit, which are located in such a way as to reduce the end corrections, are at ground potential. The outer radius plate is raised to a positive potential and the inner radius plate to an equal negative potential. To supply the required potentials (±15 kv with 0.01 percent stability), work on an electronically regulated supply was initiated. Development work was under way at the time of these experiments but the requirements on voltage steadiness had not been met. However, experience with stacks of dry cells for this purpose had shown that they were practical where the current drains were small (one or two microamperes). Figure 1 shows the arrangement of the dry cell stacks* used in this work. The 5000 volt boxes were adjustable through 20 volts and each of the other boxes were adjustable through 10 volts except for the lower 500 volt boxes which could be adjusted from 0–500 volts continuously. A fixed resistor divider of manganin was used to compare this 500 volt box against a potentiometer.

The procedure in selecting a given analyzer plate voltage is as follows: (a) Choose a combination of battery boxes that gives approximately the required voltage; (b) adjust the lower 500 volt box in each stack to 500 volts;** (c) compare and balance the next 500-volt boxes with these boxes and adjust for zero circulating current (0.2 μa was detectable); (d) add the two 500-volt boxes together and compare with the 1000-volt box and so on until the stacks have been adjusted. The total voltage may be varied over a 500-volt range by resetting the potentiometer to

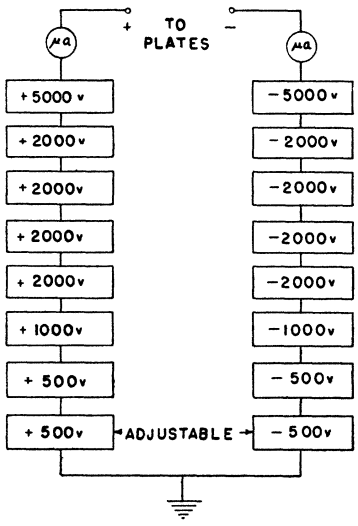

FIG. 1. Block diagram of battery stacks. Adjustable 500-volt boxes were set to any voltage below 500 volts by means of a potentiometer. The polarity of any of the boxes except the adjustable 500-volt box could be selected at will for comparison purposes.

[5] R. E. Warren, J. L. Powell, and R. G. Herb, Rev. Sci. Inst., **18**, 559 (1947).

* 5000 volt boxes used Eveready No. 493, 300 volt batteries. All other batteries were of the Burgess XX45, $67\frac{1}{2}$ volt type except for several heavier duty batteries under continuous drain to provide continuous range of adjustments.

** The actual voltage is 504.08 Int. volts and is determined by the resistor divider ratio and the 1.50000 volt setting on the potentiometer.

a chosen value and then readjusting the lower 500-volt boxes for a balance.

The limitations on accuracy in the above procedure are discussed below.

1. Accuracy of balancing battery boxes. In each box used, an off-balance voltage of 0.01 percent was easily detected. The probable error in the total voltage introduced by imperfect balancing is therefore negligible.

2. The proton beam hitting the analyzer plates. This caused a current drain from the battery stacks of 1 μa or less during most of the measurements. The current was monitored continuously during each run and corrections to the battery voltages were computed from the measured internal resistance of the batteries.

In measuring the internal resistance of the batteries an unexpected difficulty was encountered. Even new batteries, recording full voltage when checked with a voltmeter draining about 50 μa, had resistances of about 100,000 ohms per kilovolt at current drains of less than 5 μa. Older batteries, in some cases, had many times this resistance. The resistance of each stack was measured several times during the course of the experiments by drawing 3 or 4 μa from each stack in turn through high voltage resistors, and determining the corresponding shift of the yield curves as plotted against potentiometer voltage. After the completion of the experiments the internal resistance of each box of batteries was determined by balancing two nearly equal boxes and measuring with a potentiometer the change in voltage caused by a drain of one or two microamperes from one of the units. Both methods of measurement gave consistent results. Therefore, in correcting for the current drain from the battery stacks, it is estimated that the uncertainty in battery resistance can cause an error no greater than 0.01 percent.

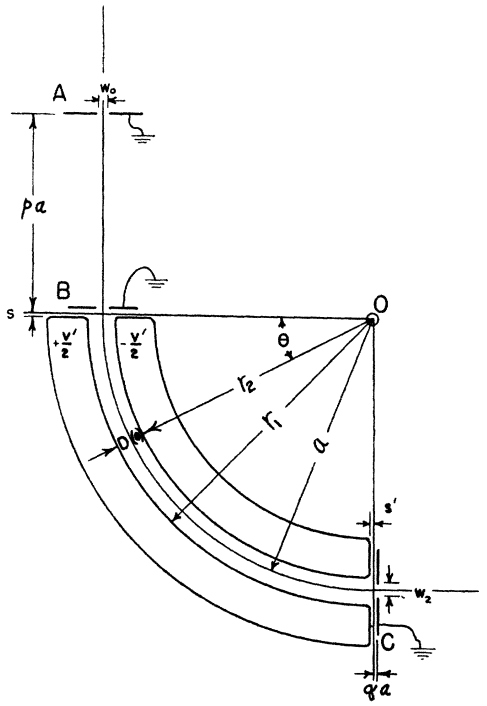

FIG. 2. Outline of electrostatic analyzer with plate separation highly exaggerated. Slits A, B, and C are the entrance slit, aperture limiting slit, and exit slit respectively. Note that p and q are dimensionless measures of the quantities they describe. Point O is the center of curvature. Distances S and S' are the distances to the effective entrance and exit planes of the analyzer from the ends of the analyzer. The angle Φ between these two planes is the total analyzer angle. Radius a is the geometric mean of r_1 and r_2. Magnetic fields are considered as positive if directed up from plane of paper.

3. Leakage currents from stacks to ground connections on battery boxes. This current was monitored with a suitably placed microammeter and at all times it was kept below $\frac{1}{2}$ μa. Taking the most unfavorable case of the first run on Li where several poor batteries were included in the stacks and the entire stack voltage ($\pm$15 kv) was used, the internal resistance amounted to about 5 megohms. This gives an error in the battery stack voltage of about 0.015 percent.

4. Drift of the battery voltage during run. This was accounted for by measuring the resulting off-balance currents in a recheck of the battery stacks after each run. The drifts were no greater than 0.01 percent and an attempt was made to correct for them by assuming a linear drift from the beginning of each run.

5. Standard cell used in potentiometer. A comparison intercheck of the standard cell used in these experiments with two auxiliary standard cells calibrated at the University of Wisconsin Standards Laboratory*** indicated that the value used was accurate to about 0.01 percent.

6. Potentiometer used to adjust variable 500-volt battery boxes. In setting up the battery stack, the two variable 500-volt boxes are first

*** Standard cells at the Wisconsin Standards Laboratory are regularly checked at the National Bureau of Standards.

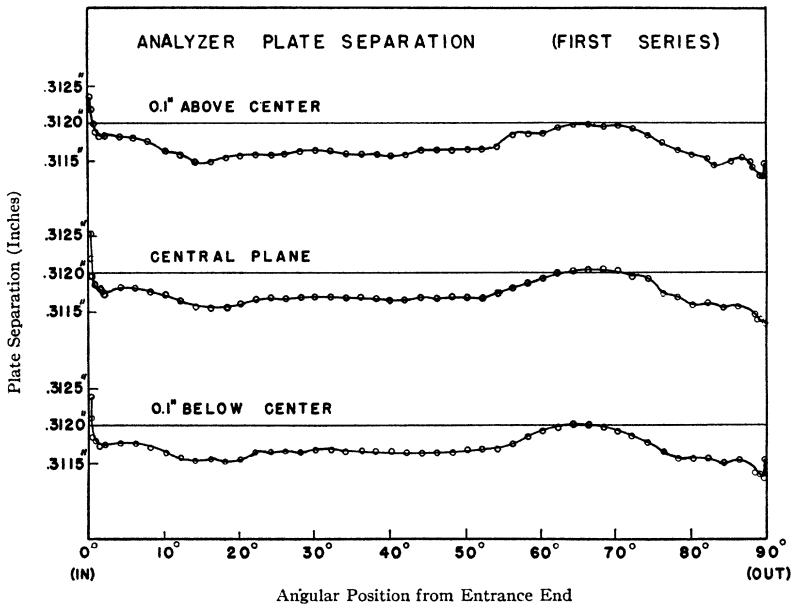

FIG. 3. Measurements of analyzer plate separation as a function of the angle θ from the analyzer entrance taken after first series of runs.

adjusted to 500 volts by means of a voltage divider and a potentiometer set at 1.50000 volts. These 500 volt values are then used as units in balancing against the other boxes; hence, any percentage error in the 1.50000 volt potentiometer setting causes the same percentage error to appear in the total battery voltage. All other settings of the potentiometer scale, which are used only to vary the two 500-volt boxes, need not be known as accurately as the 1.50000 volt point since large voltages are in series with the 500 volt boxes.

To insure the correctness of the 1.50000 volt setting, the Rubicon potentiometer used in the experiments was carefully interchecked with a Type K-1 Leeds-Northrup potentiometer. This included a check of the accuracy of transfer of the standard cell dial settings to the e.m.f. dial settings and a subsequent test of the linearity of the e.m.f. readings through the zero setting. It was concluded from these tests that the Rubicon potentiometer gave correct voltage readings within ± 0.00001 volt for any setting from 0.00010 volt to 1.50000 volts. The interval, 0.00000 to 0.00010 volt, apparently had the correct total resistance but its variation with respect to the dial setting was in error; it indicated, for instance, that the zero voltage occured at a setting of 0.00005 volt. Since an error of ± 0.00001 volt at 1.50000 volts is a negligible percentage error the percentage error at this setting is given directly by the standard cell percentage error.

7. Resistor divider used to compare the variable 500 volt boxes with the standard cell. After the measurements were completed the resistor divider was sent to the National Bureau of Standards for calibration. There the divider was studied under varying conditions of humidity over the voltage range which had been used. A change in voltage from 100 volts to 500 volts changed the ratio from 336.061 to 336.046 or 0.0045 percent. A measurement of the ratio after 23 days in a desiccator and then after 32 days in an atmosphere of 83-percent humidity indicated a change in the ratio of 0.005 percent. The Bureau's estimate of error in the ratio was 0.015 percent. Since the percentage error of each of the above effects causes an equal percentage error in the total battery voltage the net uncertainty in the battery voltage may be found by taking the square root of the sum of the squares of the above percentage errors. This gives about 0.03 percent.

GEOMETRICAL MEASUREMENT ON ANALYZER

An examination of the electrostatic analyzer theory given by Warren *et al.*[5] shows that the quantities described below must be measured (see Fig. 1).

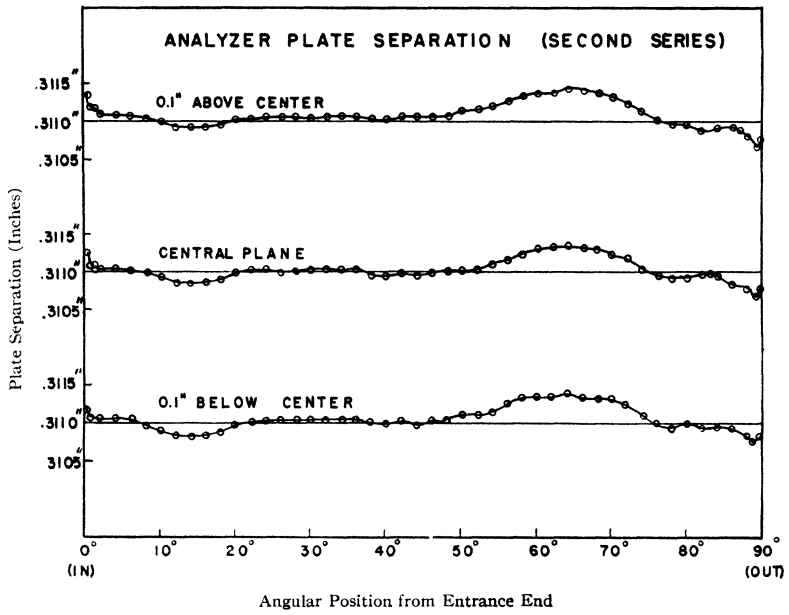

FIG. 4. Measurements of analyzer plate separation taken after second series of runs.

1. Radius of inner and outer plates. To measure the radius contour of each plate a reference gap constructed from gauge blocks was set up and aligned at the entrance end of the analyzer. Using an adjustable parallel and several combinations of gauge blocks for checking consistency, the distance between the near end of the reference gap and the pivot ("*O*" Fig. 2) was blocked out reproducibly to 0.002″ out of 40″ or to 0.005 percent. To measure the radius contour of each plate a dial gauge was mounted rigidly on a heavy bar. This bar was free to move about the central pivot "*O*" and was supported at its extremity by a wheel resting on the ground machinists' surface plate which supports the analyzer. Dial gauge readings were taken on each of the two surfaces as a function of angle at several different heights over the region of the central plane. Comparison readings on the surfaces of the reference gap were made repeatedly. These measurements were not used to determine the separation contours since a second series of measurements described below proved more dependable. They did serve as a rough check on the plate separation contours and were needed in work on the corrections to show that the effects of a tangential electric field were negligible.

2. Plate separation. A dial gauge with two contact points (something like a small inside micrometer) which directly measured the plate separation was used to measure the plate separation contours. Its mount was similar to the previous case except that it was held in a suspension which assured uniform contact pressure on both plates and measurement of the perpendicular distance between the plates. Reference gap readings were taken before and after each series of measurements at a given elevation in the analyzer gap. Figures 3 and 4 show the plate separation data taken in the central plane and 0.1″ above and below this plane for each of the two series of runs. It is seen that 0.0001″ was reproduced dependably. Since the gap was about 0.312″ the uncertainty in plate separation appears to be about 0.03 percent. There is a net reproducible fluctuation in the plate separation of about 0.0005″. This does not contribute to the error since a method of allowing for small variations in plate separation was used in the calculations.

3. Position of the centers of the entrance slit, aperture limiting slit, and exit slit. The position of the center of the entrance slit had to be known with respect to the intersection of the geometric mean plate radius and the effective plane defining the entrance to the analyzer (see Appendix I for definition of this effective plane). From (1) the geometric mean radius may be considered as known. Triangulation measurements then were made from this point and from the pivot point "*O*" to the center of the entrance slit. These

measurements were complicated by the slit container, but, after a series of careful measurements, the final uncertainty in the position of the entrance slit was estimated to give an error in the energy determination of about 0.01 percent.

The distance from the aperture limiting slit to the analyzer entrance could be measured to about 0.002″. An error in the location of this slit of this amount gives a corresponding error in the energy of 0.002 percent.

The distance from the exit slit to the exit of the analyzer plates affects the end correction in such a way as to change the magnification (see Appendix III). Since this only changes the amount of other corrections it is of second order importance.

4. Analyzer angle. The analyzer angle has an effect on the energy corrections only through the magnification, hence, as above, errors are only of second order importance.

5. Width of the opening of all slits. The slit openings, each of which could be measured to 0.001″, do not affect the mean energy determinations except in the case of the aperture limiting slit. Here an error of 0.001″ produces, through a change in the end correction, 0.0001 percent error in the energy. The effect of the opening of the slits is to give a triangular energy distribution to the proton beam at the exit of the analyzer, the total width of which is $4\cdot(300/8)\cdot(W_0/a)$ percent (see Eqs. (6) and (7)), where W_0 is the entrance slit width and a is the geometric mean radius. Thus the total energy spread is 0.075 percent of the mean energy since, in our case, $W_0=0.020''$ and $a=40''$.

6. Rounding of the corners at the ends of the analyzer plates. Since the radius of curvature of the corners (approximately $\frac{3}{16}''$) is about the same as the distance between the aperture limiting slit and the ends of the analyzer plates, it was felt that the effective position of the analyzer entrance plane might be calculated incorrectly if square corners were assumed. Appendix I gives briefly the details of the calculation, showing that the rounding effect results in a correction of only 0.001 percent.

The net uncertainty in the proton energy measurement due to the geometrical factors enumerated above is estimated to be about 0.04 percent.

MAGNETIC FIELD MEASUREMENTS

A small rectangular flip coil connected to a Leeds and Northrup Type R galvanometer was used to explore the magnetic field in the analyzer gap. Because of the low resistance of the flip coil the galvanometer was highly damped, and served as a sensitive fluxmeter (0.15 gauss per mm deflection).

Both the vertical and horizontal components of the magnetic field were measured as a function of angular position within the gap and as a function of distance between the entrance slit and the analyzer entrance. The analyzer plates were magnetized in a peculiar fashion, both components of the field reversing sign several times throughout the length of the analyzer. The average vertical component within the analyzer was 0.12 gauss upward and varied from about +0.3 gauss to −0.2 gauss. The average horizontal component was about 0.25 gauss but varied by as much as 9 gauss. The horizontal component was assumed to have no effect and the vertical component was treated as uniform, with a value equal to its average. Outside the analyzer the vertical component of the magnetic field averaged to 0.47 gauss downward. This varied from 0.35 gauss at the entrance slit to 0.61 gauss at the analyzer entrance. Again the average value was used and a uniform field was assumed. The horizontal component was less than 0.1 gauss and was also neglected.

From Eq. (2), the energy correction introduced by the magnetic field within the analyzer is about −0.008 percent for a 1 mv proton beam. Equation (4) gives +0.011 percent for the correction due to the magnetic field outside the analyzer. The total correction is then 0.003 percent and was neglected.

TARGET TECHNIQUES

In order to obtain reproducible results it was essential to maintain targets at elevated temperatures and to place a liquid air trap in the vicinity of the target.[6] In this work the targets were heated to 200°–250° Centigrade. The Li targets were prepared by evaporating lithium onto previously baked out tantalum backings. Exposure to air then permitted oxidation.

[6] R. S. Bender, F. C. Shoemaker, and J. L. Powell, Phys. Rev. **71**, 905 (1947).

The thin Al targets were prepared by evaporating known quantities of aluminum onto prepared tantalum backings. They also were exposed to air before bombardment. Oxidation was probably complete for the target of 200 volts absorption thickness but the thicker targets probably were not completely oxidized.[7] Both the thin and thick Al targets were, in reality, composite targets and a knowledge of the thickness of each layer would be necessary to determine the true resonance position from the yield curves. No correction was made for the thick target because of the unknown amount of oxide. A correction was attempted for the thin targets since these targets were either completely or almost completely oxidized. The thin target measurements should then permit an estimate of the oxide on the thick target. The data were not sufficiently consistent to give this thickness; however, each set of runs on Al was consistent to a few hundredths of a percent so it was assumed that the oxide film on the thick target did not introduce uncertainties of more than 0.02 percent.

For the fluorine target, CaF_2 was evaporated onto the tantalum backings after previously fusing it in a beryllium oxide crucible. Exposure to air was permitted before bombardment but, presumably, this did not affect the target. A fine mesh platinum gauze covered the CaF_2 crystal which was used for the thick target. This prevents an accumulation of charge on the crystal which might give an erroneous resonance energy value.[8]

EVALUATION OF PROTON BEAM ENERGY

An elementary description of the ion dynamics in the present analyzer has been given by Warren *et al.*[5] Since we are concerned with an absolute calibration the details necessary to evaluate all the corrections will be given. First, the ideal analyzer, having infinitesimal slit widths and no fringing fields will be considered relativistically. Corrections to this theory caused by improper slit alignment, finite slit width, irregular contours of analyzer plates, fringing electric fields, and the presence of a small magnetic field both inside and outside the analyzer will be calculated nonrelativistically. The ideal analyzer is considered to have an electric field determined inside by the simple equations for concentric cylinders, and outside to have zero field (i.e., no end effects and perfect radial contours). Appendix II shows that, for the conditions present in this analyzer, the relation that holds for the ideal path (i.e., radius equal to geometric mean of inner and outer radii of analyzer plates) is

$$\tfrac{1}{2}V' = V_0(1-\gamma)\frac{d}{b}, \tag{1}$$

where

$\frac{1}{2}V'$ = positive battery stack voltage (negative stack is of same magnitude),
V_0 = proton energy in volts,
d = plate separation,
b = arithmetic mean of inner and outer radii,
$\gamma = V_0(\text{mv})/1880$.

For a given physical arrangement of the aperture limiting slit and exit slit, Appendix I shows that there exist effective planes at which the electric field inside the analyzer may be thought of as terminating. Outside these planes the electric field is zero and inside it has the value determined by a geometry of two concentric cylinders. The aperture limiting slit has no effect on the passage of an ion through the analyzer other than partially determining the position of the effective entrance plane and limiting the angular spread of the beam. On the other hand, the exit slit not only determines the position of the effective exit plane but its opening partially determines the energy spread of the emergent beam.

The first order focusing theory is concerned with the motion of the particles in the neighborhood of $r=a$ (paraxial rays in optical terminology). Appendix III shows that the effect of a small vertical component of a magnetic field inside the analyzer is to change Eq. (1) into:

$$\tfrac{1}{2}V' = V_0(1-\gamma)\cdot\left(1+\frac{eaB_i}{c(2emV_0)^{\frac{1}{2}}}\right)\cdot\frac{d}{b}, \tag{2}$$

where Gaussian units are used and e is the proton charge, B_i is the vertical (positive upwards in Fig. 2) component of the magnetic induction, c is the velocity of light, a is the geometric mean radius of the plates, and m is the proton mass.

[7] Private communication, F. C. Shoemaker.
[8] E. J. Bernet, R. G. Herb, and D. B. Parkinson, Phys. Rev. 54, 398 (1938).

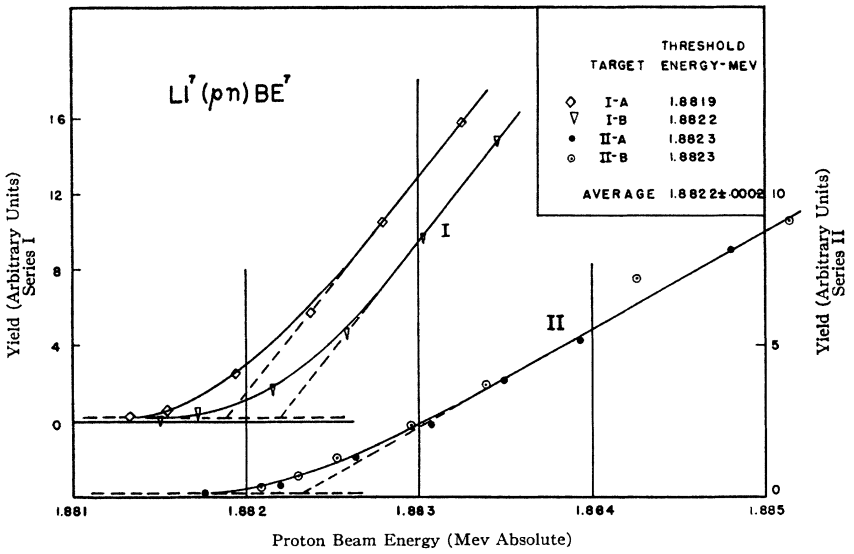

FIG. 5. Neutron yield curves for both series of measurements of Li(pn) threshold reaction.

Appendix III also shows that ϵ, the fractional correction to the energy V_0 caused by improper location of the slits and presence of a small magnetic field exterior to the analyzer, is given by Eq. (37). This may be separated into part (a), the contribution due to the improper location of the slits,

$$\epsilon_s=(2/1-M)(x_2-Mx_0), \tag{3}$$

where x_0 and x_2 measure the perpendicular distances from the ideal path of an ion to the centers of the entrance and exit slits respectively. The ideal path is taken to be the circle of radius a within the analyzer and the straight lines tangent to this circle at the effective entrance and exit planes. x_0 and x_2 are measured in units of a and are positive if they correspond to an increase in radius over the ideal radius a. M is the analyzer magnification as explained in Appendix III. Part (b), the fractional energy shift caused by the presence of the external magnetic field B_0, is given by:

$$\epsilon_m=\frac{p}{1-M}\left(\frac{\partial M}{\partial\Phi}-pM\right)\frac{eaB_0}{c(2emV_0)^{\frac{1}{2}}}, \tag{4}$$

where p is the distance between the entrance slit and the effective entrance plane measured in units of a.

The conditions necessary for Eqs. (3) and (4) to hold are that the distance between the exit slit and the effective exit plane be very small, as is the case in the present analyzer, and that the plate separation d in Eq. (2) be taken as the following weighted mean:

$$d=\frac{\sqrt{2}}{1-\cos\sqrt{2}\Phi}\int_0^{\Phi}D(\theta)\sin\sqrt{2}(\Phi-\theta)d\theta. \tag{5}$$

The fact that x_0 and x_2 in Eq. (3) should be measured to the center of the slits can be seen by considering a plot of x_2 versus x_0 with ϵ_s as a parameter. From this plot and the assumption that the number of protons per unit energy range is constant over the range of energies accepted by the analyzer, it is evident that in the general case the energy distribution at the exit of the analyzer has the form of a symmetrical truncated triangle. If, as was approximately the case in the present analyzer, the relation between the entrance slit width W_0, and the exit slit width W_2 is

$$W_2=-MW_0, \tag{6}$$

where M is the magnification ($M\cong-0.60$), then the energy distribution at the exit of the analyzer has the form of an isosceles triangle. In this case the total energy spread is given by

$$\epsilon_t=-4(M/1-M)(W_0/a). \tag{7}$$

EXPERIMENTAL PROCEDURE

The electrostatic analyzer was opened up, cleaned, and geometrical measurements were taken to estimate the difficulty in making final precise measurements. Before starting the first

series of runs, the standard cell used with the potentiometer was checked at the University of Wisconsin Standards Laboratory. Fresh targets of Li, Al, and CaF_2 were evaporated onto tantalum backings which in turn were inserted into the target chamber; a thick piece of Al and a crystal of CaF_2 covered with a fine mesh platinum gauze were also inserted with the corresponding thin targets. A number of yield curves with the first target, Li, had to be taken before consistent data were obtained. Early measurements showed that the magnitude of the internal resistance of the batteries was very large and that continuous monitoring of the current drain was required. The internal resistance of the batteries was measured after the first run on Li, after the first run on Al, and after the last run on Li, the order of the experiments being Li, Al, and F for the first series and F, Al, and Li for the second series. Reasonable estimates then were made in order to get the internal battery resistance after each run.

After the first series of yield curves were obtained (Figs. 5, 6, 7) the analyzer was opened and accurate geometrical measurements were made. Because of preliminary difficulties, extensive running time was required for these first yield curves. The ion beam bombardment had caused the formation of a hard black tarnish or deposit on the plate surfaces in the plane of the ion beam. It was felt that this deposit might seriously affect the accuracy of the measurements. The outer deflecting plate then was removed and the working surfaces of both plates were thoroughly cleaned with crocus cloth. All the tarnish and a small thickness of metal were removed in this cleaning.

The outer plate then was replaced with no attempt to duplicate the previous separation, in order to provide as completely as possible an independent set of measurements. The slits, which had been removed, now were replaced and a complete set of geometrical measurements were again taken. Fresh targets were prepared for the second series of runs which were taken with but little difficulty (Figs. 5–7). The running time was approximately a factor of 10 shorter than for the first series. An examination of the plates after completion of this work showed very little deposit on the plates. The satisfactory check obtained between the two series of runs indicates, in particular, that the deposit on the plates did not cause serious inaccuracies.

In addition, a careful exploration of the magnetic field between the analyzer plates and along the path of the ion beam from the entrance slit to the entrance of the analyzer was made with a small flip coil. Finally, the potentiometer

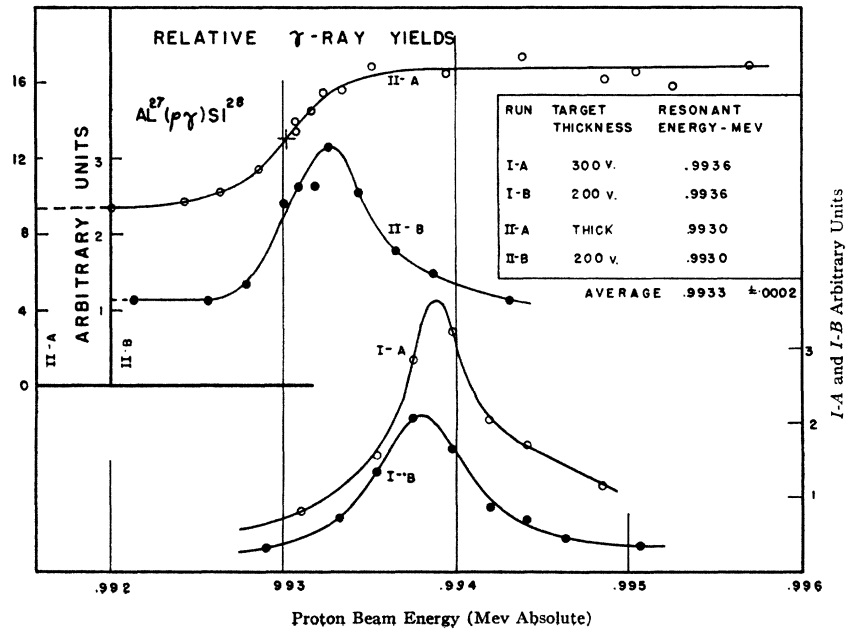

FIG. 6. γ-ray yield curves for both series of measurements of $Al(p\gamma)$ resonance reaction. Yield values are all on same relative scale.

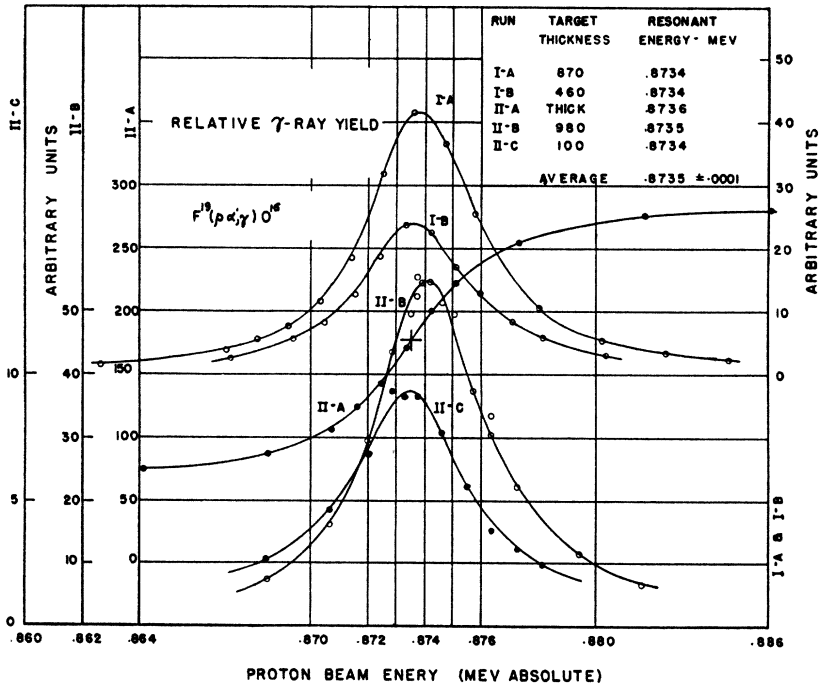

FIG. 7. γ-ray yield curves for both series of measurements of $F(p\gamma)$ resonance reaction. Yield values are all on same relative scale.

linearity was examined, the standard cell again was checked at the Wisconsin Standards Laboratory, the internal resistance of each battery box was measured at low drain, and the resistor divider was sent to the National Bureau of Standards for calibration.

EVALUATION OF DATA

The following corrections were applied to the experimental data: (1) correction for drift of the battery stack voltage, (2) correction for a change in the battery stack voltage caused by current drain from the stacks to the analyzer plates through the internal resistance in the battery stacks, and (3) correction for a shift in the resonance voltage of a thin target of finite voltage absorption thickness with respect to that of an ideally thin target of zero absorption thickness.

To convert potentiometer readings to battery stack voltages the resistor ratio for the lower 500-volt boxes as given by the Bureau of Standards was used in connection with the known number of additional battery boxes. Using the weighted mean plate separation (Eq. (5)) as found from Figs. 3 and 4 and the measured arithmetic mean radii of the plates, Eq. (1) gave the proton energies measured in volts corrected for relativistic effects and irregular contours of the plates. These voltages were then corrected for the measured deviations of the slit centers from their ideal positions (Eq. (3)) and for the magnetic fields both inside (Eq. (2)) and outside (Eq. (4)) the analyzer. Since the standard cell voltage was in international volts, all the values were increased by 0.033 percent to convert to absolute volts.

Both series of Li are shown in Fig. 5. The neutrons were counted by a BF_3 counter with about $\frac{1}{2}''$ of paraffin between the target and the counter. The finite energy spread of the proton beam accounts for the tails on the curves. If the cross section for the reaction were constant above the threshold, if the targets were uniform, and if the detector were energy insensitive, the yield curve would be linear after all the protons in the beam were energetic enough to cause the reaction. The curves do appear to have a reasonably linear portion and they were therefore extrapolated back to give the thresholds. Since the rounded tails of the curves extend over a region approximately equal to the total energy spread of the beam, this method appears to be justified. The average value of the threshold voltage for the four separate runs is 1.8822 mv where all

threshold voltages for the individual runs are within ± 0.016 percent of the average value.

Figure 6 shows the $Al^{27}(p\gamma)$ resonance. The geometrical arrangement of the target and detector was not changed between the first and second series so the thick target yield curve of the second series was used with the thin targets of the first series to calculate target absorption thicknesses. With the reservations mentioned under Target Techniques, giving an uncertainty of about 0.02 percent, the data give four independent values of the resonance energy. For the first series of two thin targets these energies are very close together giving an average value of 0.9936 mv. The second series of a thin and a thick target gives resonance energies which are also very close together with a value of 0.9930 mv for the average. The average of these two values gives 0.9933 mv for the resonance energy where all individual values are within ± 0.03 percent of this average.

Figure 7 shows the $F^{19}(p\gamma)$ resonance. In the first series two thin targets were used and in the second series a thick CaF_2 crystal was used in addition to two thin targets. Since the geometry of the detector and target was not changed between each series, the thick target was used to give the thin target absorption thicknesses for each series. The CaF_2 targets may be considered as simple targets as opposed to the composite targets of the previous case; therefore, the target absorption thickness may be calculated from much simpler considerations. The average value of the resonance energy for the five separate runs is 0.8735 mv where all individual values are within ± 0.015 percent of this value.

DISCUSSION OF RESULTS

As a basis of comparison, several measurements of reaction energies in the voltage range considered are summarized as follows:

1. Based on Tangen's[3] value of 503 kv for a weak $Al(p\gamma)$ resonance which in turn was based on Tangen's absolute measurement of 440 kv for the $Li(p\gamma)$ reaction, Broström *et al.*[9], using a generating voltmeter whose linearity was checked with H^+, HH^+, and HHH^+ ions, obtained a value of 986 kv for a prominent $Al(p\gamma)$ resonance. A very strong doublet resonance occurred at a mean value of 1.375 mv.

2. Based on a value of 440 kv for the $Li(p\gamma)$ reaction, Bernet *et al.*[8] used a generating voltmeter whose linearity was checked with H^+, and HH^+ ions, and obtained a value of 862 kv for the strong $F(p\gamma)$ resonance. Care was taken to prevent the thick target crystal, CaF_2, from charging up by placing a fine mesh gauze over the crystal.

3. Based on a value of 862 kv for the strong $F(p\gamma)$ resonance where the CaF_2 crystal was covered with a nickel gauze, Plain *et al.*,[10] using a generating voltmeter, determined a secondary calibrating point of 1.368 mv at the strong $Al(p\gamma)$ resonance. A value of 505 kv was obtained for a weak $Al(p\gamma)$ resonance and a value of 985 kv for a strong $Al(p\gamma)$ resonance.

4. Based on a value of 862 kv for the strong $F(p\gamma)$ resonance, Haxby *et al.*,[11] using a generating voltmeter whose linearity was checked with H^+, HH^+, and HHH^+ ions, obtained a value of 1.856 mv for the $Li(pn)$ threshold and a value of 2.028 mv for the $Be(pn)$ threshold.

5. Hanson *et al.*,[4] using an electrostatic analyzer for an absolute calibration, find a value of 1.883 mv for the $Li(pn)$ threshold. Using the electrostatic analyzer as a comparator they find a value of 2.058 mv for the $Be(pn)$ threshold, a value of 877 kv for the strong $F(p\gamma)$ resonance, and a value of 446.5 kv for the $Li(p\gamma)$ resonance.

6. The present results give a value of 1.8816 mv for the $Li(pn)$ threshold, a value of 873.2 kv for the strong $F(p\gamma)$ resonance, and a value of 993.0 kv for a prominent $Al(p\gamma)$ resonance. All the above values are given in international volts. Using absolute volts (1 international volt $= 1.000330$ absolute volt) the present results are 1.882 mv, 873.5 kv, and 993.3 kv for the Li, F, and Al reactions respectively.

An examination of the above results shows that there is a discrepancy of about 1.5 ± 0.5 percent between the points based essentially on the resistor stack calibration and those based on the electrostatic analyzer calibration. It is suggested that target difficulties may be responsible for the

[9] K. J. Broström, T. Tuus, and R. Tangen, Phys. Rev. **71**, 661 (1947).

[10] Plain, Herb, Hudson, and Warren, Phys. Rev. **57**, 187 (1940).

[11] Haxby, Shoup, Stephens, and Wells, Phys. Rev. **58**, 1035 (1940).

± 0.5 percent fluctuations; however, the 1.5 percent discrepancy remains unresolved.

The value of 440 kv for the Li($p\gamma$) resonance was given with an estimated uncertainty of 2 percent by Hafstad *et al.*,[1] and by Parkinson *et al.*,[2] while recently Tangen[3] has given the same value with an estimated uncertainty of about $\frac{1}{2}$ percent. Hanson *et al.*,[4] felt that their uncertainties were about 0.3 percent, whereas, in view of the over-all consistency of the thin and thick target data and the reproducibility of the electrical and the geometrical measurements, it was felt that the uncertainties of the present work were about ± 0.1 percent. However, some pertinent factor might have been overlooked, and another independent determination of these values would be desirable.

ACKNOWLEDGMENTS

The authors wish to acknowledge the generous assistance of Messrs. Dorr Ralph and Gerson Goldhaber in several phases of the work. One of us (O.S.) wishes to acknowledge the support given by the Rockefeller Foundation. The work was supported in part by the Atomic Energy Commission and in part by the Wisconsin Alumni Research Foundation.

APPENDIX I. DETERMINATION OF EFFECTIVE ENTRANCE AND EXIT PLANES OF ANALYZER

The factors influencing the position of the planes where the internal electric field may be thought of as terminating are: (a) The locations of the aperture limiting slit and exit slit, (b) the finite size of the opening in the slits, (c) the rounding of the corners of the analyzer plates, and (d) the radius of curvature of the analyzer plates. Herzog[12] has discussed effects (a) and (b). A slight but tedious modification using a rounded corner transformation[13] allows an estimate of the third effect. Since the above effects were estimated using plane parallel geometry for the analyzer plates, the effect of the radius of curvature was not investigated but probably only changes the above corrections by a fraction of the order of the plate separation divided by the radius of curvature (i.e., approximately 1 percent) and hence was neglected.

Referring to Figs. 2 and 8, let S_0 be the value of S when $r=0=w$ (i.e., for zero slit opening and no rounding of the corner). Herzog[12] then gives:

$$S_0=\frac{2d}{\pi}\tan^{-1}\frac{a}{2d}-\frac{a}{\pi}\ln\frac{2}{(1+(2d/a)^2)^{\frac{1}{2}}}. \tag{8}$$

[12] R. Herzog, Zeits. f. Physik **97**, 596 (1935).

[13] W. R. Smythe *Static and Dynamic Electricity* (McGraw-Hill Book Company, Inc., New York, 1939), p. 97.

If ΔS_w is the correction to S_0 due to small opening of the slits, then Herzog[12] gives, after approximating his exact but implicit solution:

$$\Delta S_w=\frac{\pi}{16}\cdot\frac{w^2}{a}\cdot\frac{1}{1+(2d/a)^2}\ \text{(infinitely thin slit)}. \tag{9}$$

To determine the effect of the rounding of the corners the slit may be assumed to be closed. The transformation,[13] which takes the real axis in the Z_1-plane into the approximate boundary shown in the Z-plane, is given by

$$Z=jC\int\frac{[(Z_1-1+\epsilon)^{\frac{1}{2}}+\lambda(Z_1-1-\epsilon)^{\frac{1}{2}}]\cdot[(Z_1+1+\epsilon)^{\frac{1}{2}}+\lambda(Z_1+1-\epsilon)^{\frac{1}{2}}]}{Z_1^2-a_1^2}dZ_1. \tag{10}$$

The electrical problem in the Z_1-plane is two positive line charges at $Z_1=\pm a_1$. This gives the complex potential as

$$W=U+jV=-\frac{V_0}{2\pi}\ln\left[\left(\frac{Z_1}{a_1}\right)^2-1\right]+j\frac{V_0}{2}, \tag{11}$$

where U is the stream function, V is the potential function, and V_0 is the potential difference of the analyzer plates. The integral may be evaluated in terms of elementary transcendentals. However, an approximation is used to get a relation between the constants ϵ, λ, a_1, in the Z_1 plane and the corresponding constants r, d, a, in the Z plane. If the radius of curvature of the rounding is small then a sufficient approximation is to set $\lambda=1$ and to expand all terms containing ϵ, retaining terms up to ϵ^2. Following Herzog's procedure[12] we find that the effective position of entrance to the analyzer is given by

$$S=S_0+\frac{a}{12\pi}\epsilon^2\left[1+\frac{6}{5}\left(\frac{2d}{a}\right)^2\right], \tag{12}$$

where the term in ϵ represents the rounded corner effect. The relation between ϵ and r to the first approximation is given by

$$\epsilon^{\frac{1}{2}}=\tfrac{3}{4}\pi\cdot\frac{r}{a}\cdot\frac{(2d/a)^2}{1+(2d/a)^2}. \tag{13}$$

The details of the calculation are quite tedious and are not reproduced here. However, the algebraic correctness was insured by two independent calculations using different points in the Z_1-plane to find the corresponding points in the Z-plane. Thus S_0, given by Eq. (8), together with ΔS_w given by Eq. (9) and the ϵ^2 term in Eq. (12), when added together should give a good estimate of the effective position of the entrance to the analyzer. The position of the exit slit is not very critical since it only determines the total analyzer angle. This angle only enters the corrections and hence corrections to its value can be neglected. In designing the analyzer an attempt was made to set $S_0=0$ so all the corrections are expected to be small.

APPENDIX II: IDEAL ANALYZER RELATIONS

The electrostatic potential between the plates of two concentric cylinders with a charge per unit length $+Q$ on the outer plate of radius r_1 and $-Q$ on the inner plate of radius r_2 is

$$\Psi=2Q\ln(r/a), \tag{14}$$

where $a=(r_1r_2)^{\frac{1}{2}}$, the geometric mean of the plate radii. If the inner plate has a potential $-\frac{1}{2}V'$ and the outer plate

has a potential $\frac{1}{2}V'$ each with respect to ground, then

$$V'=2Q\ln(r_1/r_2). \tag{15}$$

To find the ideal path of the ions in the analyzer, balance the centripetal force $2Qe/r$ against the centrifugal force mv^2/r and note that the kinetic energy $(m-m_0)c^2$, plus the potential energy $e\Psi$ within the analyzer, is equal to the energy eV of the ions from the generator. Making use of the fact that $m=m_0/(1-v^2/c^2)^{\frac{1}{2}}$ or its equivalent $m^2v^2=(m^2-m_0^2)c^2$ it may be seen that:

$$Q=(V-\Psi)\frac{1+[e(V-\Psi)/2m_0c^2]}{1+[e(V-\Psi)/m_0c^2]}, \tag{16}$$

which is a constant for constant radius. Thus for an analyzer with a charge Q on the plates, in order to have a constant radius for the path of an ion that enters tangentially, it must have an energy eV that differs for different points of entry depending on the potential Ψ at that point. This may be thought of as due to a variable dipole layer at the ends of the analyzer which reduces the potential to zero outside in order that the ideal problem may represent its physical counterpart. The ideal path is chosen as the one for which $\Psi=0$ or, from Eq. (14), $r=a=(r_1r_2)^{\frac{1}{2}}$. Let the corresponding generator voltage be called V_0. Then:

$$Q=V_0(1+\gamma)/(1+2\gamma), \tag{17}$$

where

$$\gamma=\frac{eV_0}{2m_0c^2}=\frac{V_0(\text{mv})}{1880}. \tag{18}$$

Using this value of Q, Eq. (15) may be expanded in powers of the small numbers γ and d/b where b is the arithmetic mean of the plate radii and d is the plate separation. This gives:

$$V'=2V_0(1-\gamma+2\gamma^2+\cdots)\left(\frac{d}{b}+\frac{1}{12}\frac{d^3}{b^3}+\cdots\right). \tag{19}$$

Since $\gamma\sim0.001$ and $d/b\sim0.01$ it follows that the higher order terms may be neglected to an accuracy of 0.001 percent. Equation (1) of the text is the result.

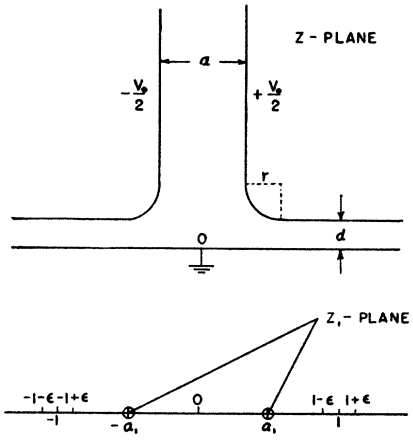

FIG. 8. Outline of quantities used in transformation of real axis of Z_1 plane into boundary shown in Z plane. Electrical problem in Z_1 plane corresponds to two positive line charges at $Z_1=\pm a_1$.

APPENDIX III: ION DYNAMICS

A non-relativistic discussion of the ion beam dynamics may be based on the following Lagrangian in polar coordinates and Gaussian units:

$$L=\tfrac{1}{2}m(\dot r^2+r^2\dot\theta^2)-e\Psi(r,\theta)+\frac{e}{c}r\dot\theta A_\theta(r), \tag{20}$$

where the potential of the ion between the analyzer plates is given by a function of the form:

$$\Psi(r,\theta)=C\ln\frac{r}{a}+\Sigma_\lambda\,(A_\lambda r^{n_\lambda}+B_\lambda r^{-n_\lambda})\cos(n_\lambda\theta+\alpha_\lambda). \tag{21}$$

The vertical uniform magnetic field is accounted for by the vector potential

$$A_\theta(r)=\tfrac{1}{2}B_i r. \tag{22}$$

Approximations will be introduced to enable the small higher order effects of the slightly non-radial contours of the analyzer plates represented by the summation to be determined. The constant C is determined from a knowledge of the ion beam energy eV_0 and the small magnetic field B_i. Since the magnetic field, the deviation of the path of the particle from $r=a$, and the angular dependence of the potential (i.e., deviation of the analyzer plates from constant radii) are all small, we may consider their effects separately.

First, consider only the effect of the small magnetic field. By Lagrange's equations, approximating for small A_θ:

$$m\ddot r-\frac{p^2}{mr^3}+\frac{eC}{r}=0, \tag{23}$$

where

$$mr^2\dot\theta+\frac{e}{c}rA_\theta=p=\text{constant}. \tag{24}$$

Since $r=a$ is to be an exact solution, then, from Eq. (23), the angular momentum that the incoming ion must have is determined by $p^2=ma^2eC$. However, the energy of a particle entering with this angular momentum is $eV_0=\frac{1}{2}ma^2\dot\theta^2$. Using Eqs. (22) and (24) with $r=a$, we see that

$$C=2V_0\left(1+\frac{eaB_i}{c(2emV_0)^{\frac{1}{2}}}\right). \tag{25}$$

Since the change in the angular momentum caused by the small magnetic field also causes a compensating change in the constant C in the electrostatic potential, the ion beam dynamics for the paraxial paths is unchanged. Therefore, the only effect of a small vertical magnetic field is to change Eq. (19) of the Appendix II into

$$V'=2V_0\left(1+\frac{eaB_i}{c(2emV_0)^{\frac{1}{2}}}\right)(1-\gamma)\frac{d}{b}. \tag{26}$$

The magnetic field effect inside the analyzer being accounted for, the path of a paraxial ion may now be calculated by setting $r=a(1+x)$ and $V=V_0(1+\epsilon)$. If the potential $\Psi(r,\theta)$ is expanded in the neighborhood of $r=a$ and third order terms are neglected, the result is

$$\Psi(x,\theta)=[2V_0+f_1(\theta)]x-V_0x^2+f_2(\theta). \tag{27}$$

To a first approximation $f_1(\theta)$ and $f_2(\theta)$ can be calculated by dropping the V_0x^2 term and requiring that $\Psi=\pm\frac{1}{2}V'$ on the plate surfaces. The torque $\partial L/\partial\theta$ may be set equal to zero for the following reasons based on its net effect: The

magnitude of the terms in θ in the potential Ψ is a measure of the gain in kinetic energy of the ions by tangential acceleration within the analyzer which is lost again as the ions pass out of the analyzer into a region of zero potential. This change in kinetic energy that occurs gradually throughout the analyzer produces a change in direction that cannot be compensated for by the opposite kinetic energy change at the exit of the analyzer. The magnitude of the terms in θ measure the amount of this deflection. A liberal estimate gives 0.005 percent for the possible energy error.

With the torque now set equal to zero, conservation of angular momentum follows and a simple differential equation of the path of the ion may be written down. If only first order effects are considered and the equation of conservation of energy is used to express the angular momentum p within the analyzer in terms of the total energy eV, the differential equation is

$$\frac{d^2x}{d\theta^2}+2x=\epsilon+\frac{D(\theta)}{d}-1. \tag{28}$$

Here,

$$D(\theta)=d-\frac{d}{2V_0}f_1(\theta) \tag{29}$$

is the actual plate separation as a function of angle and d is a weighted mean plate separation as yet to be determined. Noticing that $\alpha\cong dx/d\theta$ is the angle that the path of the ion makes with the tangent to a circle ($r=$const.) through the point and using x_1 and α_1 to denote the position and direction of the ion beam at $\theta=0$, the solution is

$$x=\tfrac{1}{2}\epsilon+\frac{1}{\sqrt{2}}\alpha_1\sin\sqrt{2}\theta+(x_1-\tfrac{1}{2}\epsilon)\cos\sqrt{2}\theta+\frac{1}{d\sqrt{2}}\int_0^\theta[D(\varphi)-d]\sin\sqrt{2}(\theta-\varphi)d\varphi. \tag{30}$$

This gives

$$\alpha=\alpha_1\cos\sqrt{2}\theta-\sqrt{2}(x_1-\tfrac{1}{2}\epsilon)\sin\sqrt{2}\theta+\frac{1}{d}\int_0^\theta[D(\varphi)-d]\cos\sqrt{2}(\theta-\varphi)d\varphi. \tag{31}$$

Since the exit slits are placed approximately at the exit of the analyzer plates, it is convenient to set the integral in Eq. (30) equal to zero for θ equal to the analyzer angle Φ. This gives:

$$d=\frac{\sqrt{2}}{1-\cos\sqrt{2}\Phi}\int_0^\Phi D(\varphi)\sin\sqrt{2}(\Phi-\varphi)d\varphi. \tag{32}$$

Thus, d is determined as a weighted mean of the separation contour data $D(\varphi)$.

Outside the analyzer, the earth's magnetic field causes the ion beam to deviate from a straight line. To a first approximation only the vertical component is effective in causing an apparent energy shift. Balancing the centripetal and centrifugal forces determines R, the radius of curvature of the ion. If the kinetic energy of the ion is expressed in terms of the beam voltage and the radius of curvature in units of a, the value of R is:

$$R=\frac{c}{eaB_0}(2emV_0)^{\frac{1}{2}}\text{ (Gaussian units)}. \tag{33}$$

If an ion enters the entrance slit at a position x_0 and at an angle α_0 to the ideal path then, because of the external vertical magnetic field, it will enter the analyzer at a position

$$x_1=x_0+\alpha_0 p+\frac{p^2}{2R} \tag{34}$$

and will now be inclined at an angle

$$\alpha_1=\alpha_0+\frac{p}{R}, \tag{35}$$

where p is the distance from the effective entrance of the analyzer to the entrance slit measured in units of a. These values of x_1 and α_1 are then to be inserted in the equations for x and α. Since the exit slit is placed very close to the effective exit plane ($q\cong 0$), a straight line path for the emergent ion may be assumed. Following Herzog[14] we may then choose the relation between the entrance and exit slits to be

$$(p+q)\cos\sqrt{2}\Phi-\sqrt{2}pq\sin\sqrt{2}\Phi+\frac{\sqrt{2}}{2}\sin\sqrt{2}\Phi=0. \tag{36}$$

An ion entering the entrance slit at x_0 will leave the exit slit at x_2 where

$$x_2=\tfrac{1}{2}\epsilon-\left(\tfrac{1}{2}\epsilon-x_0-\frac{p^2}{2R}\right)M-\frac{p}{2R}\frac{\partial M}{\partial\Phi}, \tag{37}$$

and $M=-[q\sqrt{2}\sin\sqrt{2}\Phi-\cos\sqrt{2}\Phi]$, the lateral magnification of the analyzer. The integral in Eq. (31) does not appear in Eq. (37) since it would have occurred multiplied by q and was dropped since $q\cong 0$. Furthermore, the relation between x_0 and x_2 is independent of the angle α_0 of the entering beam.

[14] R. Herzog, Zeits. f. Physik **89**, 447 (1934).